RESEARCH ARTICLE

Numerical Simulation of the Hydrodynamic Characteristics of the Porous I-type Composite Breakwater

Yongzhou Cheng[1,2], Zhiyuan Lin[1,2], Gan Hu[1] and Xing Lyu[1,2]

Abstract
Based on the three-dimensional Reynolds-averaged Navier-Stokes equation with the closure of renormalization group k-ε turbulence model and volume of fluid method, a wave-breakwater interaction numerical flume was developed to examine the wave-structure interaction of the porous I-type composite (PITC) breakwater. The transmission and reflection coefficients of the breakwater at different wave steepness H/L are quantitatively analyzed, and the wave-dissipating performance of the breakwater is compared. By changing the submerged depth of the breakwater, the velocity field, and vorticity field in the wave propagation process are analyzed, and the optimal working water depth of the new breakwater is explored. The results show that the vertical wave force on the PITC breakwater is greater than the horizontal wave force. In addition, during the wave dissipation process, the transverse baffle provided by the new breakwater destroys the trajectory of the water particle. In the interior of the wave-breaking chamber, the water that enters from the gap of the permeable plate mixes with the water entering through the bottom hole. The turbulence created by this process further dissipates the wave energy. The relative submergence depth of h/d has a great influence on the hydrodynamic characteristics. When the relative depth is large, most of the wave energy enters the breakwater, the wave energy dissipation of the breakwater is large, and the wave-absorbing effect is good. These research results provide important referential data for the study of permeable plate breakwaters.

Keywords Wave-structure interaction; Plate breakwater; Numerical simulation; Wave force; Regular wave; Hydrodynamic

1 Introduction

Plate-type open breakwaters act as an energy dissipator to protect shoreline and harbor buildings (Li et al. 2021a). Since the 1960s, scholars have been studying the energy dissipation performance of permeable breakwaters through physical model tests. Compared with previous breakwaters, perforated-plate breakwaters can prevent wave reflection and scour at the toe of breakwaters with their flexible construction (Elbisy 2017). Jarlan (1961) introduced perforated-plate breakwaters. The wave-dissipating chamber is formed between a perforated vertical wall and a solid vertical wall. Mani and Jayakumar (1995) studied the factors affecting the transmission coefficient of a perforated cylindrical breakwater. Yan et al. (1998) found that pile-foundation tier-retainer breakwaters have a good wave-dissipating effect, and the arrangement of retainers and porosity are the main factors affecting the transmission coefficient of breakwaters. Neelamani and Rajendran (2002a, 2002b) proposed inverted T-type and porous T-type breakwaters. Guenaydin and Kabdasli (2004) conducted a physical model test of regular and irregular waves on a U-type perforated breakwater. The analysis of the wave dissipation performance shows that the opening rate was the main factor affecting the wave dissipation performance. Teh et al. (2010) studied the hydrodynamic performance of a free surface semicircular perforated breakwater by analyzing the influence of density. Liu et al. (2014) investigated a submerged

---

Article Highlights

- A numerical model of PITC breakwater is proposed and compared with the results of physical tests.
- The hydrodynamic characteristics and structural stress of PITC breakwaters are further studied.
- The vorticity and velocity fields are studied, and the wave dissipation mechanism of PITC breakwaters is elaborated.

✉ Yongzhou Cheng
  chengyongzhou@163.com

1   School of Hydraulic and Environmental Engineering, Changsha
    University of Science & Technology, Changsha 410114, China

2   Key Laboratory of Water-Sediment Sciences and Water Disaster
    Prevention of Hunan Province, Changsha 410114, China

Jarlan-type breakwater, which consists of a perforated front wall and solid rear wall. They found that the wave-dissipating performance of the submerged Jarlan-type breakwater is better than that of double submerged vertical plates, and the wave forces are lower. Cheng et al. (2016) studied the wave-dissipating characteristics of a new-type porous I-type composite (PITC) breakwater through physical model tests. The proposed permeable chamber breakwater with multiple open I-plates has a good performance in linear wave dissipation. Fang et al. (2018) proposed and studied a four-layer submerged horizontal porous plate breakwater. They found that the breakwater has a good effect on the long-wave energy dissipation, and the dissipation performance can be improved by increasing the number and width of layers. Wang et al. (2016) proposed an arc-plate breakwater and studied its hydrodynamic characteristics. Based on physical model tests, Li et al. (2021b) compared the hydrodynamic characteristics of twin-arc-plate (TAP) and twin-flat plate (TFP) breakwaters. They found that the transmission coefficient, reflection coefficient, and wave pressure of the TAP breakwater were better than those of the TFP breakwater in the emerged and still water states. Gerardo et al. (2021) proposed a horizontal placement method for multiple plates in place of a single long plate and traditional breakwaters. The research results of the above scholars show that the wave damping structure of a plate breakwater is continuously being optimized. Meanwhile, the open-porous, double-layer, and multi-layer wave-absorbing structure makes the wave-structure interaction highly complicated. With the improvement of computational capacity, the numerical simulation method is suitable for the analysis of the hydrodynamic characteristics of complex structures, which provides a direction for the accurate calculation of such breakwater structures.

Wave reflection is a major problem in numerical wave simulations. Therefore, wave dissipation is the first problem to be solved in numerical simulations. At present, the Sommerfeld radiation condition in the radiation boundary is widely used in numerical wave dissipation applications. This method was first proposed and applied by Orlanski (1976). This method is suitable for dissipating small-amplitude linear waves, but it has little effect on nonlinear and random waves.

Lynett et al. (2000) used a numerical simulation to examine the dissipating performance of porous breakwaters under the action of solitary waves. Twu et al. (2002) found that the relative width and porosity are the main factors affecting the wave damping characteristics of vertically stratified porous structures under oblique waves. Aristodemo et al. (2015) proposed and developed a two-dimensional weakly compressible smoothed-particle hydrodynamics (SPH) model, and Meringolo et al. (2015) used this SPH model method to simulate the wave load and hydraulic characteristics at perforated breakwaters. Li and Lan (2018) proposed a horizontal-inclined-plate open breakwa-

ter model and studied the influence of the structure on the wave transmission coefficient. The vertical plates can effectively improve the eliminating performance of the breakwater. Based on the Reynolds-averaged Navier-Stokes (RANS) equation and volume of fluid (VOF) method, Zang et al. (2018) studied the force characteristics of a comb-type breakwater and found that the opening design at the bottom of the upper structure can effectively reduce wave pressure. Qin et al. (2019) studied the interaction between a twin-plate breakwater and freak waves. Based on the physical model and numerical simulation, Vijay et al. (2019) studied the influence of wave height, wave period, and other parameters on multiple slotted barriers. Mohammadbagheri et al. (2019) used a finite difference method to simulate the performance of a perforated breakwater under regular waves. Based on nonlinear multiple regression analysis, Binumol et al. (2020) studied the stability of a non-overtopping perforated quarter-circle breakwater. Poguluri and Cho (2021) used analytical and numerical methods to study the hydrodynamic characteristics of vertical slotted barriers in regular waves. Fu et al. (2021) conducted a numerical simulation study of the wave-dissipating performance of a submerged heaving-plate breakwater based on vortex kinematics and found that this kind of breakwater has a good effect on short and medium waves. Deng et al. (2019) studied the hydrodynamic characteristics of an oscillating-water-column breakwater through numerical methods and physical experiments. They found that the lengthening of the bottom plate and the smaller draught of the back plate can increase the energy dissipation. Other researchers, such as Gomes et al. (2020), Amaro et al. (2019), and Duan et al. (2020), also used the numerical simulation method to study the hydrodynamic characteristics of breakwaters. The above-mentioned studies have fully proved that the numerical simulation method is a powerful means to accurately characterize the wave-structure interaction.

Some achievements have been made in the numerical simulation of the permeable breakwater structure, but the research direction is mainly focused on the wave-breaking performance. Therefore, it is necessary to further study this structure. This paper presents a study on the hydrodynamic characteristics, structural stress, and wave dissipation mechanism of PITC breakwaters using a numerical simulation.

2 Model description and verification

2.1 PITC breakwater model

The PITC breakwater is a new structure type. This structure is composed of a plurality of I-type prefabricated plates, and the webs of the I-shaped prefabricated plates are perforated. Waves can be reflected multiple times in

the wave-breaking chamber between adjacent I-shaped panels to dissipate energy. The design of the open hole can reduce the transmission and reflection effectively, shield coastal waters, and ensure the safety of ships. In addition, this breakwater is light, which saves the cost. It is especially suitable for areas with poor seabed conditions. The wave-dissipating chamber of the breakwater combines the advantages of a horizontal plate breakwater and a vertical plate breakwater. The I-type plates are staggered, with a uniform gap arrangement, and combined into an independent wave-dissipating unit. Each of the two I-type prefabricated plates forms an independent wave-dissipating subunit. Multiple sub-units are combined into a multi-chamber, multi-layer wave-dissipating structure. A reasonable arrangement of the gap between the I-type prefabricated plates can effectively reduce the wave reflection in front of the breakwater. If medium- and long-period waves can be dealt with effectively and the transmission and reflection of waves can be reduced, favorable berthing conditions can be provided for ships.

In the numerical simulation process, the hydrodynamic characteristics and stress conditions of the PITC breakwater were studied by changing the opening rate of the breakwater model and adjusting the submerged depth and wave parameters. The section with the wave baffle in the first layer is permeable and is defined as section $Y1$. The wave enters the wave baffle of the second layer, which is defined as section $Y2$. The breakwater model is shown in Figure 1.
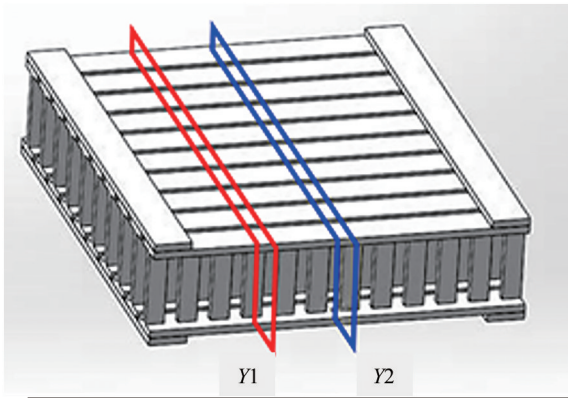

Figure 1   3D diagram of the PITC breakwater

2.2 Governing equations

2.2.1 Wave-governing equation

Continuity equation:

$$\frac{\partial}{\partial x}\left(uA_x\right) + \frac{\partial}{\partial y}\left(vA_y\right) + \frac{\partial}{\partial z}\left(\omega A_z\right) = 0 \qquad (1)$$

Momentum equation:

$$\left.\begin{aligned}
\frac{\partial u}{\partial t} + \frac{1}{V_F}\left(uA_x\frac{\partial u}{\partial x} + vA_y\frac{\partial u}{\partial y} + wA_z\frac{\partial u}{\partial z}\right) &= -\frac{1}{\rho}\frac{\partial p}{\partial x} + G_x + f_x \\
\frac{\partial v}{\partial t} + \frac{1}{V_F}\left(uA_x\frac{\partial v}{\partial x} + vA_y\frac{\partial v}{\partial y} + wA_z\frac{\partial v}{\partial z}\right) &= -\frac{1}{\rho}\frac{\partial p}{\partial y} + G_y + f_y \\
\frac{\partial w}{\partial t} + \frac{1}{V_F}\left(uA_x\frac{\partial w}{\partial x} + vA_y\frac{\partial w}{\partial y} + wA_z\frac{\partial w}{\partial z}\right) &= -\frac{1}{\rho}\frac{\partial p}{\partial z} + G_z + f_z
\end{aligned}\right\} (2)$$

where u, v, and w stand for the velocity components; A_x, A_y, and A_z, stand for the flowable-area fractions; V_F is the volume fraction; ρ stands for the density; (G_x, G_y, G_z) are the acceleration; and (f_x, f_y, f_z) are the viscous accelerations.

2.2.2 Turbulence-governing equation

The expressions of the k and ε equations, including the volume fraction V_F and flowable-area fractions A_x, A_y, and A_z, are as follows:

$$\frac{\partial k_T}{\partial t} + \frac{1}{V_F}\left(uA_x\frac{\partial k_T}{\partial x} + vA_y\frac{\partial k_T}{\partial y} + wA_z\frac{\partial k_T}{\partial z}\right)$$
$$= P_T + G_T + \mathrm{Diff}_{k_T} - \varepsilon_T \qquad (3)$$

$$\frac{\partial \varepsilon_T}{\partial t} + \frac{1}{V_F}\left(uA_x\frac{\partial \varepsilon_T}{\partial x} + vA_y\frac{\partial \varepsilon_T}{\partial y} + wA_z\frac{\partial \varepsilon_T}{\partial z}\right)$$
$$= \frac{C_1\varepsilon_T}{k_T}\left(P_T + C_3G_T\right) + \mathrm{Diff}_\varepsilon - C_2\frac{\varepsilon_T^2}{k_T} \qquad (4)$$

where P_T is the velocity gradient; G_T stands for the turbulent kinetic energy; C_1 and C_3 are 1.42 and 0.2, respectively; C_2 is calculated by K_T and P_T; and $\mathrm{Diff}K_t$ and $\mathrm{Diff}_\varepsilon$ are the turbulent diffusion terms corresponding to A_i and V_F, respectively.

2.3 Boundary conditions

Wall boundary was applied at the bottom of the numerical flume. The boundaries between the side wall and test area and the front and rear ends of the wave elimination area were set as symmetric boundaries. The upper part of the flume was set as the specified pressure boundary. The boundary at the beginning of the numerical flume was set as the wave-making boundary. The Sommerfeld radiation conditions were used to dynamically estimate the conditions of the outflow boundary. The diagram of the numerical flume is shown in Figure 2.

Based on the FLOW-3D FAVOR grid technology and the TruVOF method, a numerical water flume was established. The established numerical flume is 50.0 m in length, 0.5 m in width, and 0.6 m in height. The water depth is 0.4 m. To reduce the influence of wave reflection, a variable-step mesh porous medium was used to dissipate the wave. The uniform rectangular staggered mesh was used to establish the model mesh. The different sections of the flume were optimized using the mesh nesting tech-
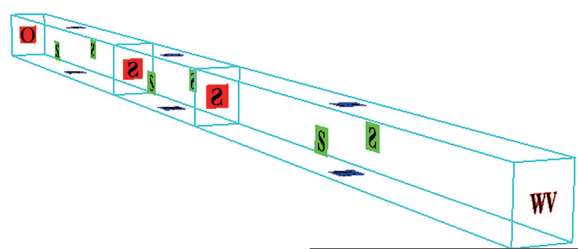
Figure 2   3D diagram of the numerical flume

Figure 3   Wave-making validation

nique. The grid size in the front-wave elimination area was set as 0.01 m. The grid size of the test area was set to 0.005 m, grid encryption was performed at the free surface, and the grid size of the encryption area was 0.001 m. The grid size of the back-end wave elimination area was set to 0.01 m. The total number of numerical flume grids was approximately 13 190 000, and a total of 144 working conditions were tested.

2.4 Verification of the numerical model

2.4.1 Wave-making validation

Hu (2016) verified the repeatability of a wave maker. In this study, the wave-making verification of the numerical flume was conducted in the same wave conditions. The adopted wave conditions are as follows: wave height H = 0.1 m and wave period T = 1.2 s. The computation is a multi-threaded parallel computation with 48 parallelisms. For each simulation, the simulation time was 30 s, and the computation time was approximately 15 to 16 h.

Figure 3 shows the wave surface duration curve of the physical test and numerical simulation. The comparison results of the two diachronic wave surface curves (t = 5 s) show that the form of the regular wave surface generated by the numerical wave flume is in good agreement with that of the physical test. The agreement between the numerical results and physical model results is more than 90%. The peak height and trough depth are the same as those of the physical test, and the wave period is very
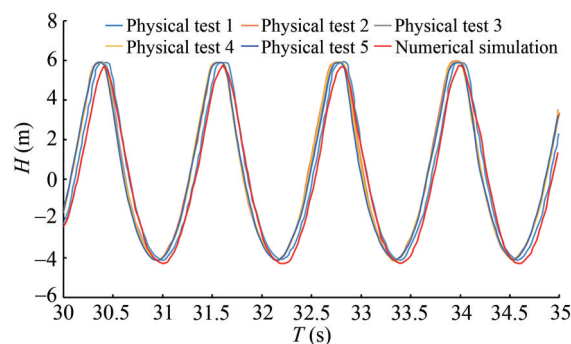
close. Hence, the wave-making of the numerical flume is verified.
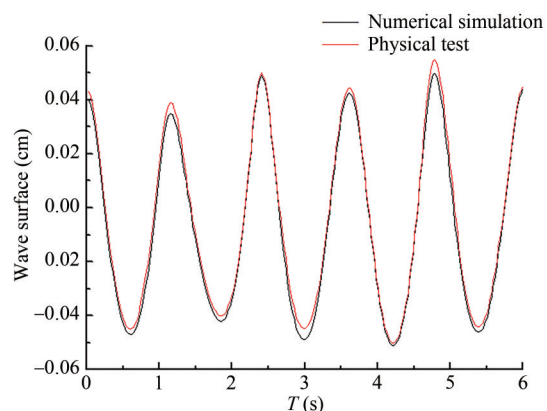
2.4.2 Wave dissipation verification

In this study, the breakwater model was placed in the numerical flume test area, and the position of the wave height measurement point was the same as that arranged in the physical test of Hu (2016).
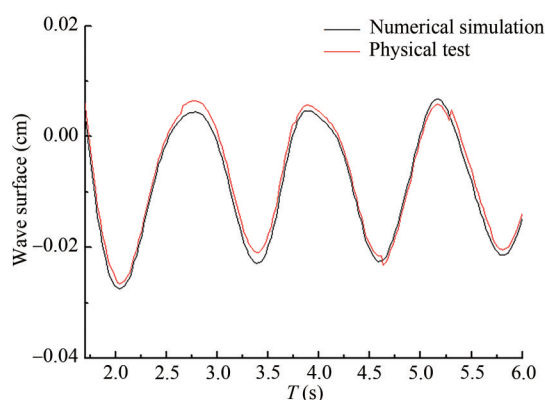
Under the same wave conditions as the physical test, the wave dissipation of the model was verified: H = 0.08 m, T = 1.2 s, D = 0.4 m, and submerged depth h is 0 m.

Figure 4(a) shows the wave surface duration curves of the physical test and numerical simulation at 2 m in front of the breakwater. The results show that the wave duration curve of the numerical simulation is in good agreement with the physical test, and the waveform is stable.

Figure 4(b) shows the wave surface duration curves of the physical test and numerical simulation at 2 m behind the breakwater. The results show that the wave height clearly decreased after the wave passed through the breakwater, the wave surface duration curve of the numerical simulation is in good agreement with the physical test, and the waveform is stable. Hence, the model selection and parameters are close to those of the physical situation, and the wave dissipation of the numerical model is verified.

(a) Wave surface duration curves at 2 m in front of the breakwater

(b) Wave surface duration curves at 2 m behind the breakwater

Figure 4   Wave dissipation verification

2.5 Test conditions

The main purpose of this study is to examine the hydrodynamic characteristics of the PITC breakwater under regular waves at different submerged depths. The model parameters are as follows: water depth d is 0.40 m, model length L_0 is 0.59 m, I-plate spacing j is 0.01 m, and spacing between the upper and lower wings of the I-plate S is 0.10 m. The model height of the breakwater is 0.12 m. The scale of the numerical model is shown in Figure 5, and the test parameters are shown in Table 1.
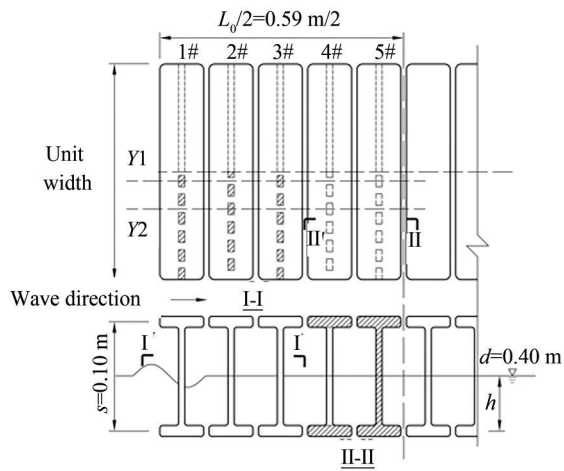

Figure 5   Schematic diagram of the breakwater model

Table 1   Numerical model test parameters

Wave height H/m	Wave period T/s	Submerged depth h/m	Relative submergence depth h/d	Opening rate A/A_0
0.08	1.0			
		0.12	0.30	
0.10	1.2			
		0.06	0.15	40
0.12	1.4			
		0	0	
0.14	1.6			

3 Results and discussions

The plate breakwater can dissipate the wave energy by destroying water particle trajectories. The adaptability of the breakwater to different wave steepness was quantified according to the variation of reflection and transmission coefficient of the breakwater under different wave steepness. The correct handling of the relationship between the breakwater elevation and free water surface is the key to determining the breakwater elevation and breakwater de-

sign. By changing the submerged depth h of the breakwater ($H = 0.1$ m, $T = 1.0$ s, 1.2 s, 1.4 s, 1.6 s; $A/A_0 = 40\%$), the flow process in the PITC breakwater was simulated. The velocity field and vorticity field with different relative submergence depths h/d were analyzed quantitatively.

3.1 Wave force

Figure 6 shows the time process curve diagram of the horizontal wave force and vertical wave force of the PITC breakwater ($d = 0.4$ m, $H = 0.10$ m, $T = 1.2$ s, $h/d = -0.15$, -0.10, 0, 0.10). Figure 6(a) shows the results of the physical test, and Figure 6(b) shows the results of the numerical simulation. The comparison shows that the numerical results are basically consistent with the physical test results.

The wave force in the horizontal and vertical directions of the breakwater periodically vmmaries, and there is a phase difference between the extreme value of the wave force in the horizontal and vertical directions.

In addition, the positive horizontal wave force is much greater than the negative wave force, indicating that the breakwater is mainly affected by the horizontal force along the wave propagation direction. The trough value of the wave force in the vertical direction is greater than the peak value, indicating that the downward wave force is greater than the upward floating force. Moreover, the wave force on the breakwater is mainly vertical downward wave force.

3.2 Influence of wave steepness

In the simulation, the Goda two-point method (Goda, 1976) was used to separate the height of the incident wave and reflected wave in front of the breakwater, and the wave surface-process measuring points were set behind the breakwater. The reflection and transmission coefficients are respectively defined as follows:

$$K_r = H_r/H_i \qquad (5)$$

$$K_t = H_t/H_i \qquad (6)$$

where H_r is the height of the reflected wave, H_t is the height of the transmitted wave, and H_i is the height of the incident wave.

The hydrodynamic performance of the new breakwater under different wave steepness H/L was compared under the following conditions: $d = 0.4$ m, $A/A_0 = 40\%$, and $h = 0.12$ m. By processing the data of the wave height, the variation of the transmission and reflection coefficients of the new-type breakwater were obtained. As shown in Figures 7 and 8, the effect of wave steepness H/L on the K_t and K_r of the breakwater is not obvious. K_t increases with the increase in wave steepness H/L under different relative water depth d/L conditions, but the growth rate is low. The
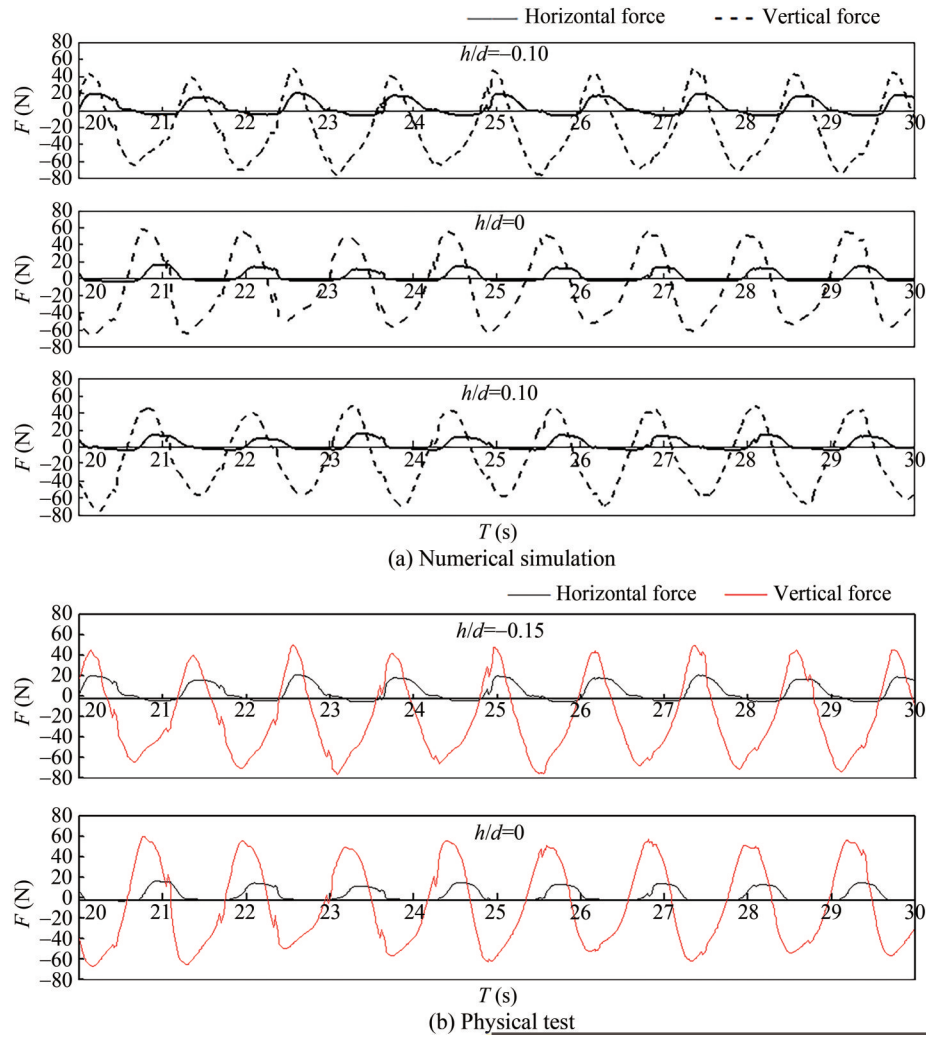
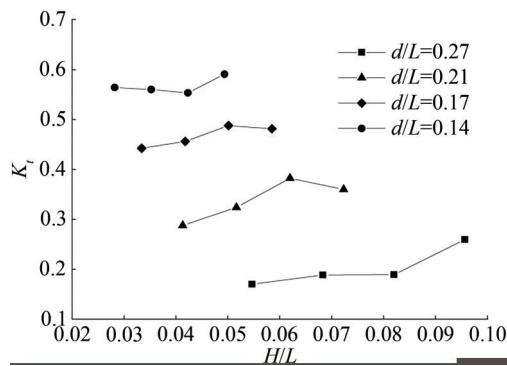**Figure 6**   Horizontal and vertical wave forces of the PITC breakwater

Figure 7   Influences of H/L on the transmission coefficient K_t

Figure 8   Influences of H/L on the reflection coefficient K_r

variation law of K_r with the increase in the wave steepness H/L is opposite to that of K_t.

3.3 Influence of the relative submergence depth on the velocity field

Figure 9 shows the velocity field distribution of section

$Y1$ of the breakwater at different relative submergence depths h/d at typical moments. When $h/d = 0.30$, the breakwater was a completely submerged flat-topped breakwater. As shown in Figure 9(a), the wave rises to the top of the breakwater, and the wave velocity is faster. During the wave movement on the top of the breakwater, part of the water enters the wave dissipation chamber through the gap
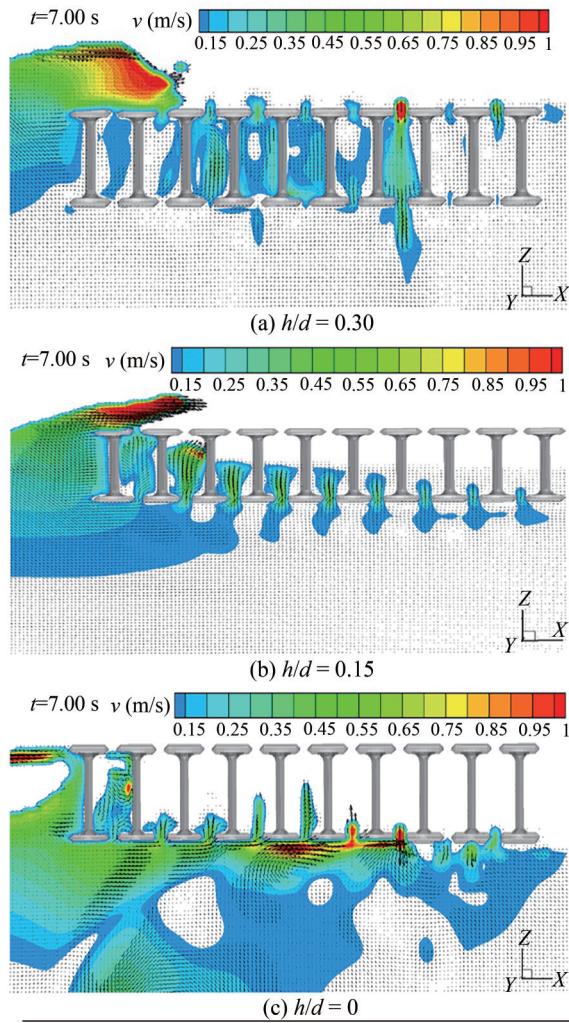
Figure 9 Contour of the velocity under various relative depths (*Y*1)

Figure 10 Contour of the velocity under various relative depths (*Y*2)

between the I-plates and flows out from the gap between the I-plates at the bottom of the breakwater.

When $h/d = 0.15$, the breakwater was a semi-submerged breakwater. As shown in Figure 9(b), a small part of the waves pass over the top of the breakwater, and most of the wave enters the wave-dissipating chamber through the permeable area. Waves collide in the wave-dissipating chamber.

As shown in Figure 9(c), when $h/d = 0$, the wave propagation is blocked by the transverse baffle of section *Y*1, resulting in a severe wave reflection. Most of the waves pass through the bottom of the breakwater, and a small amount of water enters the wave-dissipating chamber from the gap between the I-plates at the bottom of the breakwater. Hence, the absorbing effect is poor.

Figure 10 shows the velocity field cloud map of section *Y*2 under different relative submergence depths h/d at typical moments. As shown in Figure 10(a), most of the waves pass over the top of the breakwater and move toward the back of the breakwater. The water enters the wave-dissipat-
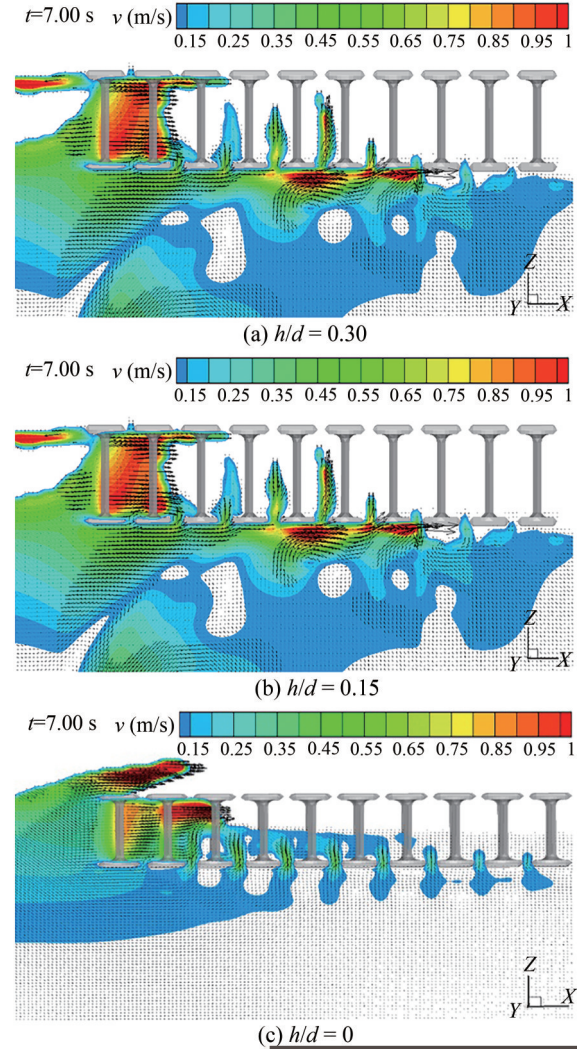
ing chamber through the porous area and interacts with the water entering the breakwater at the gap of the I-plate on the top of the breakwater. The two parts of the water move in opposite directions, and the energy of the wave dissipates.

Most of the waves enter the breakwater through the porous area, and a few waves pass over the top of the breakwater, as shown in Figure 10(b). Waves entering the breakwater through the gap at the bottom mix with the water flowing out of the breakwater and dissipate the wave energy. As shown in Figure 10(c), the waves mainly pass through the bottom of the breakwater and move toward the back of the breakwater. With a large velocity, a small amount of water enters the breakwater through the porous area and the bottom gap.

A comparison of Figures 9 and 10 shows that when h/d is 0.15, most of the wave energy enters the wave dissipation chamber, the wave energy dissipation of the breakwater is the largest, and the wave-dissipating effect is good.

As a result, the relative submergence depth has a significant influence on the velocity field. In the wave movement process, the transverse baffle destroys the water particle movement, producing pressure difference and affecting the flow velocity. With the PITC breakwater located under the still water surface, the dissipation performance is better than that produced from the PITC breakwater located above the still water surface, and more water enters the wave chamber to mix and dissipate energy.

3.4 Influence of the relative submergence depth on the vorticity field

Figure 11 shows the vorticity contour of section $Y1$ at different h/d of the breakwater at typical moments. As shown in Figure 11(a), when $h/d = 0.30$, the top of the breakwater is flushed with the water surface, and the breakwater is submerged. Most of the waves pass over the top and propagate to the end of the breakwater. The vorticity was concentrated in the wave dissipation chamber.
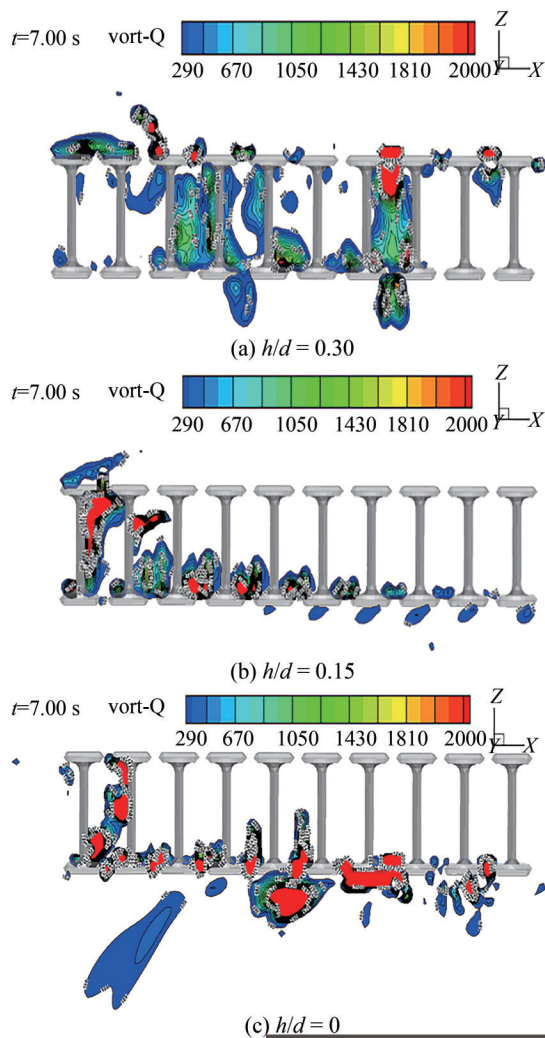
When $h/d = 0.15$, the top of the breakwater exceeds the water, and the breakwater is half out of the water, as shown in Figure 11(b). The vorticity is mainly concentrated at the bottom of the I-plate gap and the vorticity value decreases in the horizontal direction. Due to the action of gravity, the water body through the bottom gap into the wave dissipation chamber moves back and forth, resulting in turbulence and vortex.

In Figure 11(c), when $h/d = 0$, the bottom of the breakwater is flushed with the water surface, and the breakwater is all out of water. The waves mainly pass through the bottom of the breakwater, and a small part enters the breakwater. The vorticity is mainly generated by the part of the water that enters the breakwater through the bottom gap after the interaction between the surface water and the bottom of the breakwater. Because the surface velocity of the wave is the maximum, the vorticity value in Figure 11(c) is generally larger than that in Figure 11(b).

Figure 12 is the vorticity contour of section $Y2$ at differ-

(a) $h/d = 0.30$

(b) $h/d = 0.15$

(c) $h/d = 0$

Figure 11   Contour of the vorticity under various relative depths ($Y1$)

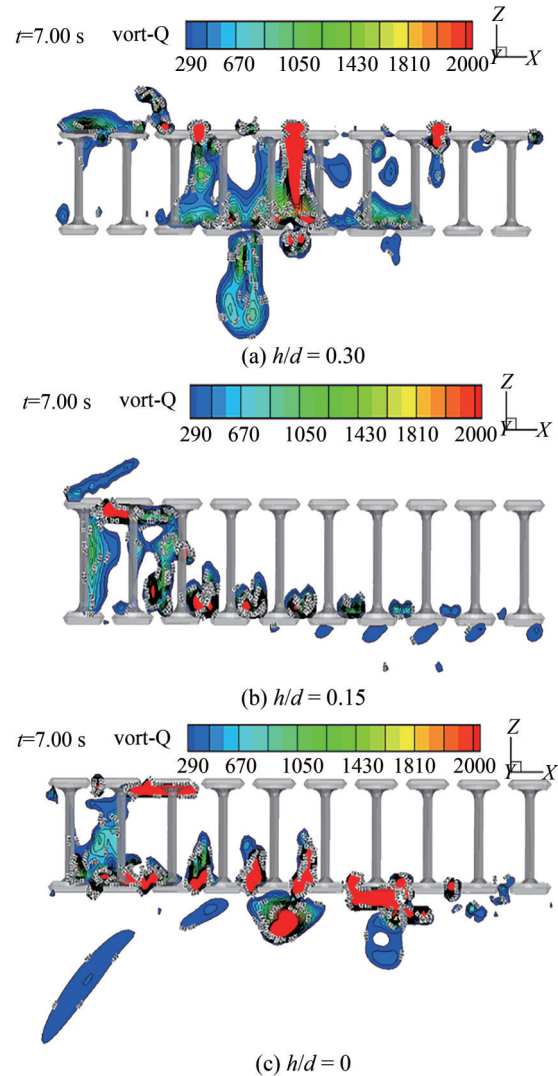(a) $h/d = 0.30$

(b) $h/d = 0.15$

(c) $h/d = 0$

Figure 12   Contour of the vorticity under various relative depths ($Y2$)

ent h/d of the breakwater at typical moments. Compared with Figure 11, the vorticity position in Figure 12 has not changed, but the vorticity value has increased. This is because section $Y2$ is the permeable area of the breakwater, with water moving in the horizontal direction, which intensifies the turbulence and increases the vorticity.

The vorticity value in Figure 12(c) is generally larger than that in Figure 12(b). This is because the velocity of the surface wave is faster, and there is a sudden change.

As a result, when the wave passes through the breakwater, the vorticity is mainly concentrated at the I-plate gap, especially at the bottom of the breakwater. The vorticity is mostly concentrated below the I-plate gap, and there are more vorticities in the wave-absorbing chamber.

3.5 Analysis of the wave dissipation process

Figure 13 shows a 3D flow velocity contour of the interaction between waves and breakwaters within one period under the following conditions: water depth $d = 0.4$ m, opening rate $A/A_0 = 40\%$, relative submergence depth $h/d = 0.15$, wave height $H = 0.10$ m, and wave period $T = 1.2$ s.
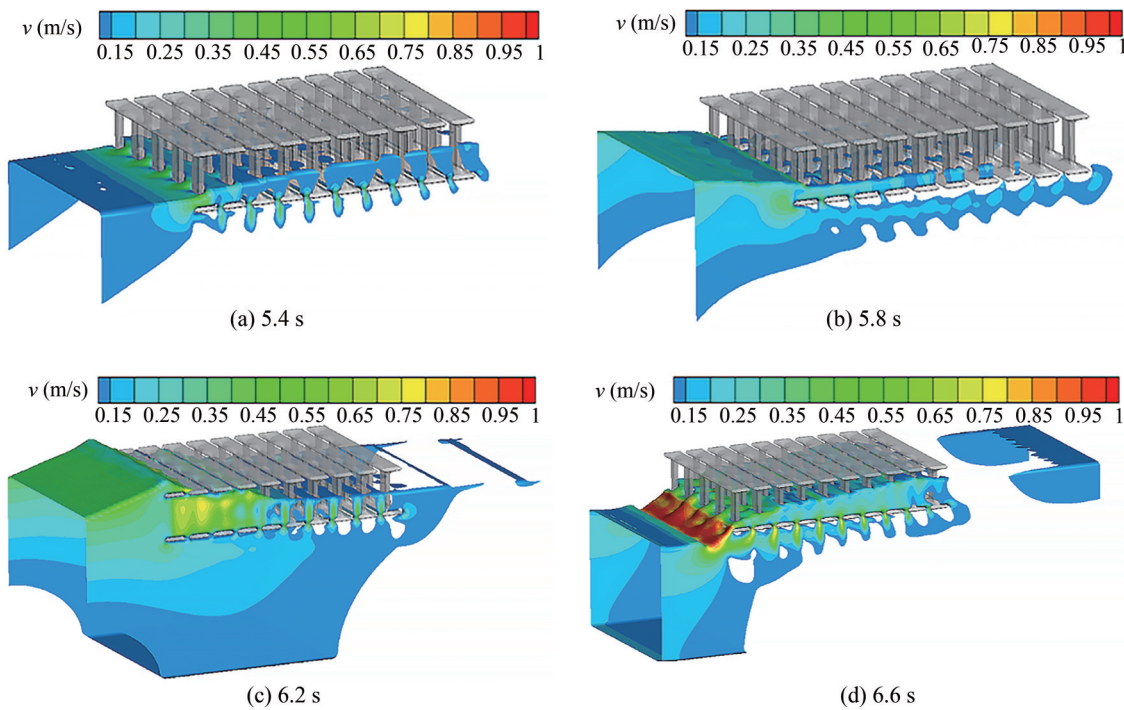

(a) 5.4 s

(b) 5.8 s

(c) 6.2 s

(d) 6.6 s

Figure 13 3D contour of the velocity in the wave-absorbing process

As shown in Figure 13(a), when waves pass through the breakwater, the flow velocity is large at the gap between the first I-plate transverse baffle and the bottom I-plate in the direction of the wave facing, and some water passes through the gap between the I-plates.

Figure 13(b) shows that the flow velocity in the permeable area of the breakwater is large, and the velocity is slow when it is closer to the position behind the breakwater.

As shown in Figure 13(c), the velocity of the wave significantly increases after it enters the breakwater, but it gradually slows down inside the breakwater.

Figure 13(d) shows a contour of the flow velocity after passing through the whole breakwater. The water in the front of the breakwater flows back to the front of the breakwater due to gravity, and the velocity is relatively large. The water behind the breakwater and the gap between the I-plates at the bottom also appears as a backflow phenomenon and flows to the front of the breakwater.

4 Conclusions

In this study, the RANS equation and VOF free surface tracking method were used to establish a numerical wave flume. The hydrodynamic characteristics of the PITC breakwater under different wave steepness H/L and different relative submergence depths h/d were examined and analyzed. The flow velocity and vorticity distribution when the wave interacts with the breakwater structure is discussed, and the 3D analysis of the wave dissipation process is performed to reveal the wave dissipation mechanism of the breakwater. The main conclusions are as follows:

The wave force of the PITC breakwater periodically changes. Wave forces on the breakwater are mainly positive horizontal wave forces and vertical downward wave forces. The effect of the vertical wave force is greater than that of the horizontal wave force.

The wave dissipation mechanism of the PITC breakwater is mainly energy dissipation. The vorticity of waves passing through the breakwater is mainly concentrated at the gap of I-plates, especially at the bottom gap of the breakwater.

The relative submergence depth h/d has a great influence on the hydrodynamic characteristics around the breakwater. When the relative submergence depth is large, most of the wave energy enters the breakwater, the wave energy dissipation of the breakwater is great, and the wave dissipation performance is good.

The velocity of the wave increases after it enters the breakwater and gradually decreases in the wave propagation process inside the breakwater. When waves pass through the breakwater, the water in the front of the breakwater appears backflow, and the flow velocity is large. After the wave passes through the whole breakwater, the water in front of the breakwater, behind the breakwater, and at the gap between the I-plates at the bottom, all appears backflow and flows to the front of the breakwater. The variation trend of the velocity and vorticity i s consistent— the greater the velocity, the greater the vorticity. Inside the breakwater, the greater the velocity of water, the greater the vorticity.

The PITC breakwater has good adaptability to complex terrain and is conducive to water exchange. The structure is light and the cost is low, which can play a good shielding effect. Moreover, it can be used in projects with poor terrain conditions and water exchange demand. However, the long-period wave dissipation effect of the PITC breakwater proposed at present is not good, and it needs to be further optimized, particularly the layout of the transverse baffle, to improve its long-period wave dissipation effect.

References

Amaro RA, Cheng LY, Rosa SV (2019) Numerical study on performance of perforated breakwater for green water. Journal of Water Way, Port, Coastal, and Ocean Engineering 145(6): 04019021.1-04019021.19. DOI: 10.1061/(ASCE)WW.1943-5460.0000528

Aristodemo F, Meringolo DD, Groenenboom P, Schiavo AL, Veltri P, Veltri M, Zhou JG (2015) Assessment of dynamic pressures at vertical and perforated breakwaters through diffusive SPH schemes. Mathematical Problems in Engineering 2015(Pt. 3): 305028.1-305028.10. DOI: 10.1155/2015/305028

Binumol S, Rao S, Hegde AV (2020) Multiple nonlinear regression analysis for the stability of non-overtopping perforated quarter circle breakwater. Journal of Marine Science and Application, 19 (2): 293-300. DOI: 10.1007/s11804-020-00145-3

Cheng, YZ, Hu G, Lu XH, Yi L, Chang JF (2016) Experimental study on wave dissipation and wave force of the porous I-type plate composition breakwater. Journal of Changsha University of Science and Technology (Natural Science), 13(2): 61-69. DOI: 10.3969/j.issn.1672-9331.2016.02.011

Deng ZZ, Ren X, Wang LX, Wang P (2019) Hydrodynamic performance of a novel oscillating-water-column breakwater with a horizontal bottom-plate: Experimental and numerical study. Ocean Engineering, 187: 106174. DOI: 10.1016/j.oceaneng.2019.106174

Duan WY, Liu RZ, Chen JK, Ma S (2020) Hydrodynamic analysis of floating breakwater with perforated structure based on the Taylor expansion boundary element method. Ocean Engineering 200: 107040. DOI: 10.1016/j.oceaneng.2020.107044

Elbisy MS (2017) Wave interactions with multiple semi-immersed Jarlan-type perforated breakwaters. China Ocean Engineering 31 (3): 341-349. DOI: 10.1007/s13344-017-0040-3

Fang ZC, Xiao LF, Kou YF, Li J (2018) Experimental study of the wave-dissipating performance of a four-layer horizontal porous-plate breakwater. Ocean Engineering 151: 222-233. DOI: 10.1016/j.oceaneng.2018.01.041

Fu D, Zhao XZ, Wang S, Yan DM (2021) Numerical study on the wave dissipating performance of a submerged heaving plate breakwater. Ocean Engineering 219: 108310. DOI: 10.1016/j.oceaneng.2020.108310

Gerardo VZM, Hector GN, Javier OTF, Edgar M, Ivan E, Ernesto TO (2021) Ocean surface waves propagating over a spatial arrangement of subsurface fixed horizontal plate breakwaters crowned with flexible medium. Journal of Fluids and Structures 100: 03188. DOI: 10.1016/j.jfluidstructs.2020.103188

Goda Y, Suzuki Y (1976) Estimation of incident and reflected waves in random wave experiments. Proceedings of 15th Conference on Coastal Engineering, Honolulu, HawaiI, 828-845.

Gomes A, Pinho J, Valente T, Carmo JS, Hegde AV (2020) Performance assessment of a semi-circular breakwater through CFD Modelling. Journal of Marine Science and Engineering 8(3): 226. DOI: 10.3390/jmse8030226

Guenaydin K, Kabdasli MS (2004) Performance of solid and perforated U-type breakwaters under regular and irregular waves. Ocean engineering, 31: 1377-1405. DOI: 10.1016/j.oceaneng.2004.02.002

Hu YC (2016) Experimental study on wave dissipation and wave force of the porous I-type plate composition breakwater. Master thesis, University of Science and Technology, Changsha, 10-11

Jarlan E (1961) A perforated vertical wall breakwater. The Dock and Harbour Authority, 41(186), 394-398

Li CL, Lan XJ (2018) Numerical simulation of wave dissipation property of a new-type open breakwater. Journal of Hydro-Science and Engineering (4), 75-80. DOI: 10.16198/j.cnki.1009-640X.2018.04.011

Li XY, Wang LX, Wang Q, Xie T, You ZJ, Song KZ, Xie XM, Wan X, Hou CY, Wang YK (2021a) A comparative study of the hydrodynamic characteristics of permeable twin-flat-plate and twin-arc-plate breakwaters based on physical modeling. Ocean Engineering, 219: 108270. DOI: 10.1016/j.oceaneng.2020.108270

Li XY, Li Q, Wang Q, Hou CY, Song KZ, Xie T, Zhang ZH, Wan X, Xie XM, Wang YK (2021b) Numerical and experimental investigation on the hydrodynamic characteristics of an arc-shaped plate-type breakwater under the action of long-period waves. Ocean Engineering 219: 108198. DOI: 10.1016/j.oceaneng.2020.108198

Liu Y, Xie LQ, Zhang ZH (2014) The wave motion over a submerged

Jarlan-type perforated breakwater. Acta Oceanologica, Sinica 33(5), 96-102. DOI: 10.1007/s13131-014-0471-0

Lynett P, Liu P, Losada I (2000) Solitary wave interaction with porous breakwaters. Journal of waterway, Port, Coastal, and Ocean Engineering 126, 314-322

Mani JS, Jayakumar S (1995) Wave transmission by suspended pipe breakwater. Journal of Waterway, Port, Coastal, and Ocean Engineering 121(6): 335-338. DOI: 10.1061/(ASCE)0733-950X (1995)121:6(335)

Meringolo DD, Aristodemo F, Veltri P (2015) SPH numerical modeling of wave-perforated breakwater interaction. Coastal Engineering 101: 48-68. DOI: 10.1016/j.coastaleng.2015.04.004

Mohammadbagheri J, Salimi F, Rahbani M (2019) Applying finite difference method to simulate the performance of a perforated breakwater under regular waves. Journal of Marine Science and Application 18(3), 314-324. DOI: 10.1007/s11804-019-00095-5

Neelamani S, Rajendran R (2002a) Wave interaction with '⊥'-type breakwaters. Ocean Engineering 29, 561-589. DOI: 10.1016/ S0029-8018(01)00030-0

Neelamani S, Rajendran R (2002b) Wave interaction with T-type breakwaters. Ocean Engineering 29: 151-175. DOI: 10.1016/ S0029-8018(01)00030-0

Orlanski I (1976) A simple boundary condition for unbounded hyperbolic flows. Journal of Computational Physics 21, 251-269. DOI: 10.1016/0021-9991(76)90023-1

Poguluri SK, Cho IH (2021) Analytical and numerical study of wave interaction with a vertical slotted barrier. Ships and Offshore Structures 16(9), 1012-1024. DOI: 10.1080/17445302.2020.1790299

Qin H, Mu L, Tang WY, Hu Z (2019) Numerical study of the interaction between peregrine breather based freak waves and twin-plate breakwater. Journal of Fluids and Structures 87, 206-227. DOI: 10.1016/j.jfluidstructs.2019.04.003

Teh H, Venugopal V, Bruce T (2010) Hydrodynamic performance of a free surface semicircular perforated breakwater. Coastal Engineering Proceedings 1(32): 1-13. DOI: 10.9753/icce.v32.structures. 20

Twu SW, Liu CC, Twu CW (2002). Wave damping characteristics of vertically stratified porous structures under oblique wave action. Ocean Engineering, 29, 1295-1311. DOI: 10.1016/S0029-8018 (01)00091-9

Vijay KG, Neelamani S, Sahoo T (2019) Wave interaction with multiple slotted barriers inside harbour: Physical and numerical modelling. Ocean Engineering 193: 106623. DOI: 10.1016/j. oceaneng.2019.106623

Wang GY, Ren B, Wang YX (2016) Experimental study on hydrodynamic performance of arc plate breakwater. Ocean Engineering 111, 593-601. DOI: 10.1016/j.oceaneng.2015.11.016

Yan YX, Zheng JH, Zeng XC, Xie HD (1998). Characteristics of wave dissipation for pile-foundation tier-retainer breakwaters. Ocean Engineering, 16(1), 67-74. DOI: 10.16483/j.issn.1005-9865.1998.01.008

Zang Z, Fang Z, Zhang N (2018) Flow mechanism of impulsive wave forces and improvement on hydrodynamic performance of a comb-type breakwater. Coastal Engineering 133: 142-158. DOI: 10.1016/j.coastaleng.2017.12.010